HLADH-catalyzed synthesis of β-amino acids, assisted by continuous electrochemical regeneration of NAD+ in a filter press microreactor

Rossmery A. Rodríguez-Hinestroza, Carmen López, Josep López-Santín, Cheikhou Kane, M. Dolors Benaiges, Théodore Tzedakis

HLADH-catalyzed synthesis of β-amino acids, assisted by continuous electrochemical regeneration of NAD^+ in a filter press microreactor

Rossmery A. Rodríguez-Hinestroza[a], Carmen López[a,1], Josep López-Santín[a,*], Cheikhou Kane[b], M. Dolors Benaiges[a], Theo Tzedakis[c,**]

[a] *Bioprocess Engineeering and Applied Biocatalysis Research Group, Departament d'Enginyeria Química, Escola d'Enginyeria, Universitat Autònoma de Barcelona, 08193 Bellaterra, Catalunya, Spain*
[b] *Laboratoire d'Electrochimie et des Procédés Membranaires, Ecole Supérieure Polytechnique, Université Cheikh Anta Diop, B.P. 5085 Dakar Fann, Senegal*
[c] *Laboratoire de Génie Chimique, UMR CNRS 5503, Université Toulouse III-Paul Sabatier, 31062 Toulouse Cedex 04, France*

Keywords:
Electrochemical NAD^+ regeneration
Electrochemical microreactor
Horse-liver alcohol dehydrogenase
β-amino acids
β-alanine synthesis, simulation

A B S T R A C T

This work focuses on the use of electrochemical microreactors, applied to the direct electroregeneration of nicotinamide dinucleotide (NAD^+) used in-situ for the enzymatically-assisted oxidation of the β-alanine. Mechanistic and chemical/electrochemical reactor approaches were investigated, to achieve satisfactory conversions (> 80%) of the substrate in reasonable (1–2 days) reaction times; no fouling observed of the gold anode. An original method was proposed to limit the complexation effect of the produced β-alanine to the enzyme. Simulations of the overall system were achieved and an estimation of the required kinetic and Michaelis constants was proposed.

1. Introduction

The regeneration of nicotinamide cofactors is a crucial step for an economic use of redox enzymes for industrial syntheses (Chenault et al., 1988, Hollmann et al., 2006, van der Donk and Zhao, 2003, Zhao and van der Donk, 2003). Cofactor regeneration simplifies product isolation, prevents problems of product inhibition by the cofactor, and can drive thermodynamically unfavorable transformations by coupling favor regeneration reactions.

Whereas regeneration of the reduced forms of the pyridine nucleotide (NAD(P)H) cofactors has been extensively investigated, recycling of $NA(P)D^+$ has been less studied. Even so, various in situ regeneration methods have been investigated (Hummel and Kula, 1989, Iwuoha and Smyth, 2003).

Electrochemistry is a promising tool for the regeneration of the different cofactors and coenzymes. Several advantages can be found as the supply of redox equivalents is basically mass-free, since only electron transfer reactions are involved; no co-substrate is required and no co-product is formed, the use of a second enzyme can be avoided, electrons are among the cheapest redox equivalents available (Kochius et al., 2012, Hollmann et al., 2010) and the technique is quite environmentally friendly.

The electrochemistry of the redox system $NAD(P)^+$/NAD(P)H has been extensively studied (Gorton and Domínguez, 2007). Direct anodic /oxidation of NAD(P)H generally occurs at high overpotentials, on which the electrode material has a significant influence (Blaedel and Jenkins, 1975; Samec and Elving, 1983). Although dimerization of the intermediate radical species has been reported (Gorton and Domínguez, 2007), since the dimer is oxidized to enzymatically active $NAD(P)^+$, this side-reaction does not limit the applicability of direct anodic $NAD(P)^+$ regeneration. To avoid the high overpotential required for the direct electrochemical oxidation of NAD(P)H, various chemical mediators can be used as electron carriers.

Microreactors were proven to be useful in a wide range of applications, mainly for process miniaturization to catalytic screening, process intensification (Pohar and Plazl, 2009), and on-site and on-demand production of chemicals (Tudorache et al., 2011). Because their reduced channel dimensions, they offer high surface area to volume ratio that allows numerous advantages such as: enhancement of the mass and heat transfers, high conversion rate and reduced energy demand.

An interesting application of microreactors is cofactor regeneration. The feasibility of continuous electroregeneration of NADH in a filter-press microreactor using FAD/$FADH_2$ as a redox mediator was

* Correspondence to: Departament d'Enginyeria Química, Biològica i Ambiental, Escola d'Enginyeria, Edifici Q-Despatx QC/1099, Campus de la UAB, 08193 Bellaterra, (Cerdanyola del Vallès), Barcelona, Catalunya, Spain.
** Correspondence to: Laboratoire de Génie Chimique, Bât. 2RI, porte 126, Université Toulouse III-Paul Sabatier, 118, route de Narbonne, 31 062 Toulouse Cedex 9, France.
E-mail addresses: Josep.Lopez@uab.cat (J. López-Santín), tzedakis@chimie.ups-tlse.fr (T. Tzedakis).
[1] Present address: Department of Chemistry and Food Technology. E.T.S.I. Agrónomos. Universidad Politécnica de Madrid, 28040 Madrid, Spain.

http://dx.doi.org/10.1016/j.ces.2016.10.010

Nomenclature

A	absorbance
l	UV cell length
C	concentration (mol/m^3)
CbA	Cbz-β-alanine or Cbz-β-amino propionaldehyde (product)
CbP	Cbz-β-amino propanol (substrate)
CE	counter electrode
CV	cyclic voltammetry
D	diffusion coefficient (m^2/s)
E	potential (V)
EA	enzymatic activity or enzyme concentration (U/cm^3)
EμR	electrochemical microreactor
F	Faraday's constant (96,500 C/mol)
FAD	flavin adenine dinucleotide oxidized form
FADH2	flavin adenine dinucleotide reduced form
HLADH	enzyme 'horse-liver alcohol dehydrogenase'
Ilim	limiting current=nFSDC/δ (A)
k^o	intrinsic heterogeneous electronic transfer constant (m/s)
k_j	kinetic constant of the step j
K_j	equilibrium constant of the step j (L/mol or without unit)
K_{Mj}	Michaelis constant of the step j (mol/L or without unit)
n	exchanged electron number
NAD^+	nicotinamide dinucleotide oxidized form
NADH	nicotinamide dinucleotide reduced form
Q	volumetric flows (m^3/s)
r	potential scan rate (V/s)
r_j	chemical rate of the step j (mol/L/h)
U	1 unit of HLADH activity (the amount of enzyme that converts 1 μmol of NADH/min)
WE	working electrode
S	Surface area (m^2)
SCE	saturated calomel electrode
t	time (s),
T	temperature (°C)
TFA	trifluoro-acetic acid
TTN	total turnover number=produced moles of CbA per mole of cofactor (for durations allow the cancellation of the concentration of the substrate).
V	volume (m3)
X_j	conversion of the specie j (%) $X_j = \frac{moles\ number\ of\ j\ transformed}{total\ moles\ number\ of\ j}$
y_f, y	faradaic yield (%) and selectivity (or Cumulative selectivity inside the batch reactor storage tank): $y = \frac{UV\ measured\ concentration\ of\ j}{[j]^o - [j]_{storage}\ \tan k}$)

Greek letters

α	anodic transfer coefficient
δ	thickness of diffusion layer (m)
ε	molar extinction coefficient ($M^{-1}\cdot cm^{-1}$)
η	overpotential (V)
λ	wavelength (nm)
ξ	proportionality constant (A.L/mol)
τ	residence time within the filter-press electrochemical microreactor: $\tau = \frac{V_{E\mu R}\ (\approx 4.10^{-8} m^3)}{Volumetricflow} \rightarrow 0.5 \leq \tau_{(s)} \leq 25$, for the fixed flow range (0.1–5 cm^3/min)
ω	angular velocity (rpm)

experimentally demonstrated (Cheikhou and Tzedakis, 2008, Choban et al., 2007, Kane, 2005, Tzedakis et al., 2010, 2016; Yoon et al., 2005). In addition, an indirect method for the electrogeneration of NADH has been developed since the direct reduction of NAD^+, leading to enzymatically inactive products, is not selective (Kane, 2005, Cantet et al., 1996, Jaegfeldt, 1981). Owing to the advantages of the use of the microreactors and the proven applicability to the regeneration of nicotinamide cofactors (NADH), an evaluation of the ability of these devices to the anodic regeneration of NAD^+ in enzyme-catalyzed oxidations is proposed in the present study, using horse-liver alcohol dehydrogenase (HLADH) as case study.

HLADH (EC 1.1.1.1) catalyzes the oxidation of α-amino alcohols with nonpolar side chains, such as L-leucinol, L-phenylalaninol, and L-valinol (Andersson and Wolfenden, 1982) and could potentially be used to synthesize α-amino aldehydes, precursors of valuable chemicals like aminopolyols (Ardao et al., 2011). In general, HLADH catalyzes the reversible interconversion of a wide variety of aldehyde/alcohol substrate pairs and the disproportionation and oxidation of aldehydes (Dalziel and Dickinson, 1965, Hinson and Neal, 1975). Based on this fact, attained aldehydes could easily oxidize, leading to the corresponding amino acid as sole product (Ardao et al., 2011). These characteristics of the oxidation of amino alcohols by HLADH, incites the consideration of their direct oxidation to the corresponding β-amino acids, by use of an enzyme that is able to recognize β-amino alcohols as substrate. β-amino acids are 1,3-difunctionalized compounds, used as intermediates in the design and construction of novel biologically and medicinally interesting molecules (Cheng et al. 2001, Juaristi and Lopez-Ruiz, 1999). They are also able to mimic the secondary structure of natural peptide sequences (peptidomimetics), and this feature facilitates interactions with receptors and enzymes and prevents peptidase degradation (Cheng et al. 2001, Steer et al., 2002). β-amino acids are useful as chiral auxiliaries, chiral ligands, chiral building blocks and intermediates in the synthesis of β-lactams (Liu and Sibi, 2002).

Although β-amino acids can be obtained using different chemical or chemoenzymatic methods (Juaristi and Lopez-Ruiz, 1999, Liu and Sibi, 2002, Rudat et al. 2012, Ege and Wanner, 2008), their enzymatic synthesis (HLADH-catalyzed) from β-amino alcohols is worthwhile to explore because of its relative simplicity and also the possibility to propose a continuously electroregeneration process for the pyridinic cofactor.

The aim of this paper is to examine the in-situ electrochemical regeneration of the NAD^+ cofactor in a plug flow type microreactor, applied for the synthesis of Cbz-β-alanine (here represented by CbA) from Cbz-β-amino propanol (here represented by CbP). Scheme 1 presents the overall reaction involved in this coupled system.

2. Materials and methods

2.1. Chemicals

Cbz-β-amino propanol (CbP, Carbo benzoxy amino *propanol*), Cbz-β-alanine (CbA), Cbz-β-amino propionaldehyde, NADH and NAD^+

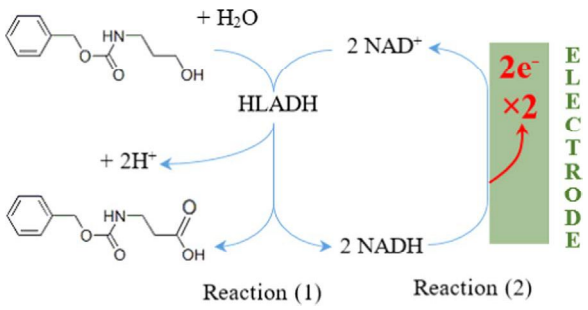

Reaction scheme 1. Indirect electro-enzymatic oxidation of the Cbz-β-amino propanol to the corresponding acid (Cbz-β-alanine), catalyzed by the HLADH enzyme, mediated by the cofactor NAD^+, which is regenerated by anodic oxidation.

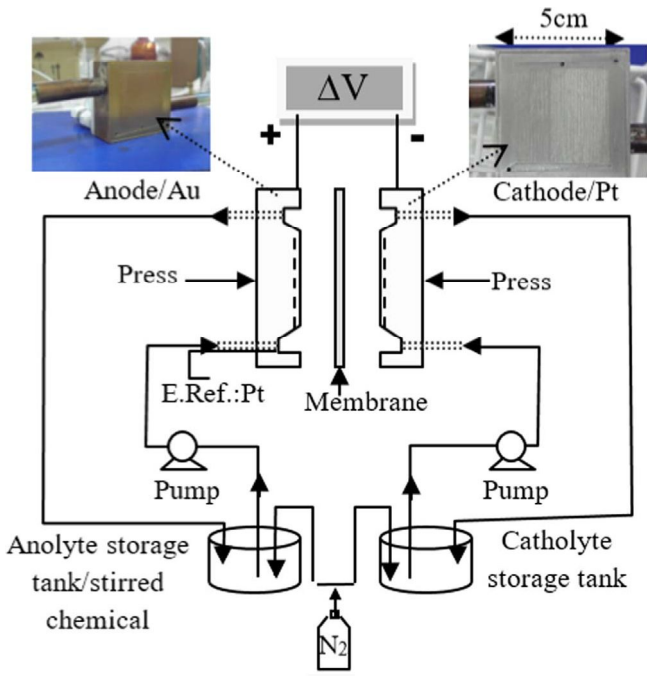

Fig. 1. Schematic representation of the divided Filter-press microreactor and both the anodic and cathodic flow circuits, used to carry out preparative electrolyses. On the top/left: Picture of the gold microgrooved cathode indicating the heat exchanger; On the top/right: Picture of the platinum microgrooved anode.

were purchased from Sigma Aldrich. For all other common chemicals the highest commercially available grade was used.

Horse-liver alcohol dehydrogenase (HLADH) was obtained from a horse-liver (purchased from a horse slaughterhouse), by extraction according to a modification of the method detailed by Dalziel (Dalziel, 1961, Rodríguez-Hinestroza, 2014). The partially purified HLADH was stored at −20 °C.

2.2. Electrokinetic studies

The electrochemical behavior of the compounds involved in the NADH oxidation was examined using a three-electrode classical electrochemical cell, at room temperature (20–22 °C), controlled by an EGG Potentiostat Galvanostat. The working electrode WE (anode) was a rotating disk (platinum or gold) polished before each experiment (abrasive suspension of alumina 1 μm). Platinum, used as a counter electrode CE (cathode), was burned in advance. The electrode potentials were measured with respect to a saturated calomel electrode SCE (reference electrode: RE) immersed in a Luggin capillary located near (~3 mm) to the rotating disk. The current-potential (I vs E) curves were plotted for all the compounds involved in the oxidation of CbP. NADH solutions were protected from light and sodium pyrophosphate buffer was used to adjust the pH of all solutions to 8.7. The examined range for potential scan rates was $20 < r_{(mV/s)} < 200$ in the case of cyclic voltammetry without stirring. Current-potential curves were plotted at the steady state (r=5 mV/s), both on the rotating disk anode ($500 \leq \omega_{(rpm)} \leq 5000$) and also in the electrochemical microreactor (EμR described in the following section), before electrolysis, under various conditions.

2.3. Preparative electrolyses

The multichannel filter-press microreactor patented by (Choban et al., 2007; Tzedakis et al., 2004, 2006, 2010), that performs the regeneration of NADH (reduction of NAD^+), was used in the present study to carry out the electrochemical oxidation of NADH (Fig. 1). The microreactor is constituted of two micro-grooved rectangular plates (5 cm×5 cm×0.2 cm) made of platinum and gold; both of them were evaluated as working electrode materials and the best material was chosen for preparative electrolyses. Each electrode has about 150 hemicylindrical microchannels (l=3 cm, r~75 μm) that allow the operating volumetric flows in the range from 0.1 to 5 cm^3/min. Both the WE anode and the CE cathode are separated by a nafion cationic membrane (N1135). A platinum wire, inserted within the inlet anodic compartment, was used as a pseudoreference electrode. Two large trapezoidal channels, located at the bottom and at the top of the metal plate, provide uniform distribution of the electrolyte to all microchannels as well as uniform output of the electrolyzed solutions (Tzedakis et al., 2014). In addition, each electrode includes, on the rear side, a heat exchanger which allows operation under the desired temperature.

The microreactor was connected to a Watson Marlow 2055 peristaltic pump. 75 or 100 mM sodium pyrophosphate buffer pH at 8.7 was used as catholyte. For continuous mode electrolyses, analyses of the electrolyzed solution were achieved after 5–10 residence times. The set-up of Fig. 1 was used for various experiments under various conditions, particularly for NADH oxidation alone (2) or coupled with the oxidation of CbP (1), in the presence (or not) of HLADH. Electrochemical regeneration of NAD^+ was achieved into the microreactor and the enzymatic reaction takes places in the bulk (batch reactor, here the anolyte storage tank, Fig. 1). For enzymatic oxidation of CbP (1), coupled with electrochemical regeneration of NAD^+ (2), a total volume of 10 mL of a stirred solution was used at 25 °C; the mixture contains CbP (18.7 mM), NAD^+ (37.4 mM) and 100 U of HLADH /cm^3, dissolved in 100 mM sodium pyrophosphate buffer at pH 8.7. The enzymatic reaction (1) proceeded for 2 h without connection to the microreactor, allowing enough production of NADH for the electrochemical oxidation (2). Furthermore, both anolyte (reaction mixture) and catholyte (buffer) were pumped into the microreactor at 1 mL/min. When operating under galvanostatic conditions, the applied current was $0.8 \times I_{lim}$ (see the following sections for the determination of the limiting current of the NADH oxidation). The indirect oxidation (1)+(2) was also performed following the same procedure as in the batch configuration, but sequential additions of the solid substrate CbP were performed (fed-batch operation mode); in fact, each time that its concentration in the mixture became lower than 10 mM, a mass was added in order to restore its initial concentration.

The advancement of the reactions was continuously monitored by determination of the concentration of the various compounds (reagents-products, enzymatic activity (EA) of HLADH). The analytical procedure is presented in the following section.

2.4. Oxidation of CbP catalyzed by HLADH without cofactor regeneration

Batch enzymatic oxidation was performed by dissolving Cbz-β-amino propanol (18.7 mM, the maximum solubility) and NAD^+(37.4 mM) in 100 mM sodium pyrophosphate buffer of pH 8.7. The reaction was initiated when HLADH was added to the mixture to reach 100 U/mL in a final volume of 5 mL, and was performed at 25 °C under stirring and protected from light. The progress of the reactions was continuously monitored as indicated above.

Fed-batch reaction of Cbz-β-amino propanol at an initial substrate concentration corresponding to the maximum solubility was initiated, using an excess of NAD^+(112.2 mM) corresponding to three times the stoichiometric one. Pulses of solid Cbz-β-amino propanol were added when the concentration decreased ≈5 mM in order to restore the initial substrate concentration. The reaction was performed using mechanical stirring and its progress was monitored as above-mentioned. Continual monitoring was performed by measuring the concentration of Cbz-β-amino propanol, the formed Cbz-β-alanine by HPLC, and the enzymatic activity by HLADH activity assay.

Table 1
Molar extinction coefficients of NADH and NAD^+ in 100 mM sodium pyrophosphate buffer pH 8.7 at room temperature..

Compound	Wavelength (λ/ nm)	Molar extinction coefficient (ε/ M^{-1} cm^{-1})	
		Experimental (Rodríguez-Hinestroza, 2014)	Bibliography (Hald et al., 1975)
NADH	340	5.58×10^3	6.22×10^3
	260	14.41×10^3	14.10×10^3
NAD^+	260	16.49×10^3	17.40×10^3

2.5. Quantification of NADH and NAD^+

Both the concentrations of NADH and NAD^+ were determined by UV–Vis spectrophotometry, according to the Beer-Lambert Law ($A = \varepsilon \cdot l \cdot C$), and using a Hewlett Packard 8452 A Diodes array spectrophotometer. Calibration curves were plotted at 340 nm for NADH and 260 nm for NAD^+(Cheikhou and Tzedakis, 2008). Table 1 summarizes the molar extinction coefficients (ε) of the involved compounds. The comparison between the obtained and reported (Hald et al., 1975) molar extinction coefficients of NAD^+ and NADH indicate similar values with a low average error percentage (Δε=5%). To monitor the concentration of the cofactor during the enzymatic oxidation of CbP (1) alone, or coupled with NAD^+ regeneration, the absorbance at 340 nm was used to estimate the [NADH]; the [NAD^+] was deduced by simple difference ([NAD^+]=[NAD^+]°- $[NADH]_{340\ nm}$). Note that this procedure does not enable knowing whether side reactions take place, nor if inactive forms of the cofactor were produced.

2.6. Quantification of substrates and products by HPLC

The concentration of the carboxybenzyl (Cbz) protected compounds: CbP, Cbz-β-amino propionaldehyde, and CbA was measured by HPLC. A Dionex Ultimate 3000 with a reversed-phase column X Bridge C18, 5 µm, 4.6×250 mm Waters was employed. The separation was achieved at 30 °C; the mobile phase was composed of two solvents: solvent A: trifluoroacetic acid (TFA) in H_2O 0.1% (v/v) and solvent B: TFA in a mixture of H_2O: acetonitrile (1:4) 0.095% (v/v). The samples were eluted at a flow rate of 1 mL/min using a gradient from 20% to 36% of the solvent B for 25 min. Samples of 30 µL were injected, and peaks were detected at the specific wavelength for each compound. Quantification was performed from peaks areas by the external standard method based on a prior calibration. Note that HPLC measurements in the involved conditions led to relatively important uncertainties which could reach 10%.

2.7. HLADH enzymatic activity assay

Horse-liver alcohol dehydrogenase activity was spectrophotometrically determined by monitoring the decrease of the NADH concentration at 340 mM when benzaldehyde was reduced to benzyl alcohol, following the in-house protocol established by Evocatal (Düsseldorf, DE). A sample of 0.05 mL was added to the mixture, which contains 50 mM triethanolamine buffer pH=7, 3 mM benzaldehyde and 0.25 mM NADH (previous incubation at 30 °C), in a final volume of 1 mL. The reaction was carried out at 30 °C for one minute. One unit of HLADH activity is defined as the amount of enzyme that converts 1 µmol of NADH per minute.

3. Results and discussion

3.1. Selection of the electrode material for direct NADH oxidation

The current-potential curves, plotted for both platinum and gold disk anodes, for NADH oxidation in the presence (or not) of the CbP substrate and the CbA product are indicated in Fig. 2. The objective is to check the influence of both the CbP and CbA, on the magnitude of the oxidation current of NADH, as a function of the electrode material.

Curves 1 (a and b), exponentially shaped for both Pt and Au anodes, represent the residual current (water oxidation); oxidation is faster on platinum (it starts at 1 V) than gold (oxidation for E > 1.2 V). The overvoltage required for the water oxidation on gold is higher than this one on the platinum, thus the gold electrode appears more appropriated for the NADH oxidation, however both Pt and Au materials will be checked.

Curves 2 (a and b), obtained with a solution of 15 mM CbA, do not exhibit any additional signal, indicating the absence of electro reactivity of this adduct. However, especially for platinum, the magnitude of the residual current decreases, and the curve of the blank shifts to higher anodic potentials. This behavior is typically representative of adsorption of CbA on platinum. Gold exhibits less affinity for CbA.

Oxidation of NADH (5 mM) on platinum is indicated by the curve 3, a; it clearly indicates that oxidation of NADH starts at 0.4 V and exhibits a plateau for E > 0.75 V, showing a diffusion-limited current attributed to the NADH oxidation (reaction 2, scheme 1). The addition of 15 mM CbP to this solution, (curve 4, a) does not significantly change the shape of the curve, meaning that i) CbP is electroinactive, and ii) the oxidation of NADH is not affected by the CbP substrate. The slight increase observed in the magnitude of the limiting current (ΔI_{lim}

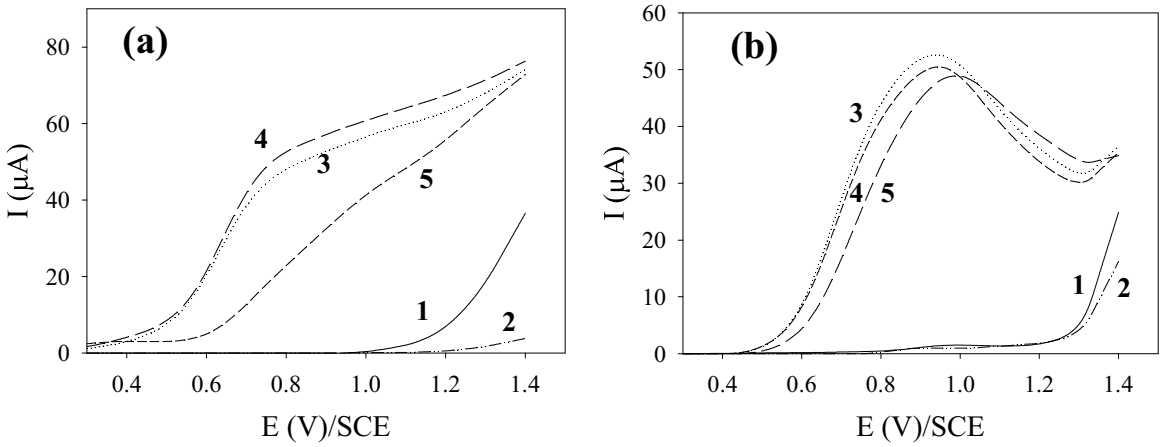

Fig. 2. Current-potential curves obtained at the steady state on a rotating disc ω= 1000 rpm, r=5 mV/s; room temperature. (a): platinum disc anode (S=3.14 mm^2); (b): gold disc anode (S=3.14 mm^2); Counter electrode: Pt; $V_{electrochemical\ cell}$=25 cm^3. 1: residual current (100 mM sodium pyrophosphate buffer pH=8.7); 2: (1) +15 mM Cbz- β-alanine; 3: (1) +5 mM NADH; 4: (3) +15 mM CbP; 5: (3) +15 mM CbA.

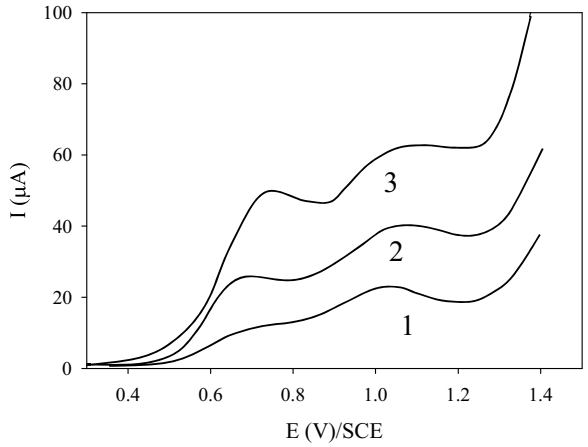

Fig. 3. Current-potential curves obtained on a gold disc anode (S=3.14 mm^2) at room temperature and transient state without convection/ω=0. Electrolyte: 100 mM sodium pyrophosphate buffer pH 8.7. 15 mM NADH; (1), (2), and (3): at 50, 100 and 200 mV/s respectively.

~5%), could be caused by a slight regeneration of NADH by the enzymatic reaction (1).

A stronger effect on the oxidation of NADH was observed after the addition of 15 mM of the CbA (curve 5, a); its adsorption on platinum, causes a decrease in the magnitude of the NADH oxidation current, and the curve was shifted to higher overvoltages. The presence of CbA makes the NADH oxidation more difficult/more irreversible, meaning that during the coupled oxidation of CbP on the platinum, the CbA product must be removed from the solution to avoid the passivation of the electrode.

The gold exhibits different behavior to that observed for the platinum; Even the NADH oxidation (curve 3, B, Fig. 2) starts at the same potentials (~0.5 V), the obtained curve exhibits a peak-shaped signal (instead the expected plateau corresponding to the mass transfer limitation, as observed for the platinum). The magnitude of the peak current observed is in the same order as the limiting current obtained on platinum. The decrease in the current observed for E > 0.9 V, translates its partial deactivation. This fact indicates that, during preparative electrolyses, the potential of the anode must be maintained at values lower than ~1 V, to avoid side reactions. The addition of 15 mM CbP (curve 4, b) or the addition of 15 mM (CbA, curve 5, b) do not significantly change the shape of the curves (ΔI_{lim} < 5%), meaning that oxidation of NADH on the gold is not affected by these compounds. The NADH oxidize at similar potential/current values on both gold and platinum anodes; nevertheless, gold material will preferred rather than the Pt; indeed the observed current is not affected by the product nor the substrate (there is no significant adsorption nor passivation when the anodic potential is maintained at values lower than 1 V). Consequently, gold was retained as anodic material for NADH oxidation for the preparative electrolysis on the microreactor, taking special care for the potential of the anode during the electrolyses.

3.2. Determination of the electrokinetic parameters of NADH on gold anode by cyclic voltammetry (CV)

The anodic behavior of NADH was examined on gold at the transient state. Fig. 3 shows the curves I=*f*(E) obtained (without stirring) for various potential scan rates in the range from 50 to 200 mV/s. Curves clearly indicate the oxidation of NADH, starting from 0.4 V, as already observed at the steady state.

All curves exhibit two distinct signals, peak shaped and centered at ~0.6/0.8 and ~1.0/1.3 V respectively, meaning that two different oxidations arose. The magnitude of the current for peaks 1 and 2 has a linear dependency on the square root of the potential scan rate (3), indicating a mass transfer limited phenomenon:

$$I_{peak\ 1(\mu A)} = 169 \times r^{0.5}_{(V/s)}\ \ R^2 = 0.996 \ \text{ and } \ I_{peak\ 2(\mu A)} = 176 \times r^{0.5}_{(V/s)} R^2 = 0.999 \quad (3)$$

The very similar slopes (Δ *slopes*/*slope* < 4%) obtained for both signals means that the same electron number is exchanged for each oxidation of NADH.

Two possibilities can be forward: i) these two peaks correspond to two different NADH groups, each one involving 2e^- (the first one being attributed to the NAD^+ formation), and ii) each peak corresponds to a monoelectronic oxidation, the final product being NAD^+. Preparative electrolyses in the next sections will help to select the appropriate reaction.

A linear correlation between the first peak potential and the natural logarithm of the potential scan rate was found:

$$E_{peak\,(V)} = 0.83 + 0.046\ \ln (r)_{rinV/s} \quad R^2 = 0.99 \quad (4)$$

The anodic transfer coefficient is deduced from the slope of the Eq. (4); its value ($\alpha n_{lim.step}$=0.27) is slightly lower than the one obtained for the electrochemical oxidation of NADH using glassy carbon (0.35) and platinum (0.45) electrodes at pH 7 (Moiroux and Elving, 1980). Combining Eqs. (3) and (4) allows the diffusion coefficient of NADH to be estimated. The obtained value (D_{NADH}=1.1·10^{-10} m^2/s) is close to the one reported by Moiroux and Elving (1980) (2·10^{-10} m^2/s).

Taking into account the determined value of '$\alpha n_{limstep}$' and the diffusion coefficient, the intrinsic heterogeneous electronic transfer constant was calculated for the first step of oxidation, that being k°=2.2 m/s, which is practically the same as that obtained by Moiroux and Elving for a bare electrode. This value indicates that the electrochemical oxidation of NADH appears to be a relatively slow electrochemical system (Tzedakis et al., 2010).

3.3. Oxidation of NADH in a filter-press microreactor

The current-potential curve obtained with the microreactor for the oxidation of 20 mM NADH at a steady state is shown in Fig. 4. A first signal appears as a peak (at E_{peak}≈0.69 V/Pt wire pseudoreference), followed by a plateau (0.9–1.1 V; I=~6 μA) which is attributed to the oxidation of NADH to NAD^+. The high specific area of the microreactor

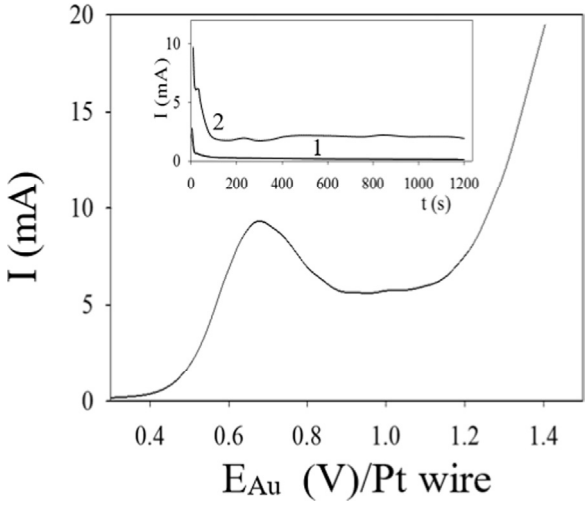

Fig. 4. Current-potential curve obtained for NADH oxidation using a filter-press microreactor (described in Fig. 1); gold anode S_a=18 cm^2; Pt cathode S_c=18 cm^2. Anolyte: 20 mM NADH in 75 mM sodium pyrophosphate buffer pH 8.7. Catholyte: 75 mM sodium pyrophosphate buffer pH 8.7. T=40 °C. $Q_{anolyte}$=$Q_{catholyte}$=50 μL/min; r=5 mV/s. **Inset:** Temporal evolution of the current, during preparative potentiostatic electrolyses. The anolyte is continuously recycled in the filter-press microreactor. Applied anodic potential: (1): E_{peak}; (2): 1 V.

enables obtaining high conversions of the NADH during one residence time (it acts as a thin layer); this causes the current to decrease because of a partial depletion of the concentration (in spite of the flow) and explains the peak shape (instead of an entire diffusion plateau) of this anodic signal. Another explanation of the peak-shaped curve could be partial adsorption, on the electrode surface, of electrogenerated products or intermediates, arising when the oxidation of NADH takes places at high potentials; fouling of the electrode has indeed already been reported by the bibliography (Aizawa et al., 1975, Blaedel and Jenkins, 1975a, 1975b, Samec and Elving, 1983); nevertheless this adsorption appears to be weak because the current in the potential range from 0.8 to 1.2 V is constant, thus favoring the assumption of concentration depletion. Preparative electrolyses (under potentiostatic conditions) were carried out in order to examine the effect of the applied potential dependence on the conversion of NADH at a steady state. The electrolyses were performed i) at the peak potential (0.69 V) and ii) at 1 V/Pt wire pseudo-reference (this last value was reported by Samec and Elving (Samec and Elving, 1983), for 20 min and the current temporal evolutions were indicated in the inset of Fig. 4.

The cumulative overall conversion of NADH (the anolyte is continuously recycled in the storage tank) at the end of the electrolyses was determined by the UV measurement of the concentration of NADH. Conversion remains low (9%) for electrolyses performed at E_{peak}; an increase in the applied potential to 1 V allows a practically full conversion (92%) of the NADH to NAD^+, demonstrating that, under the chosen conditions, oxidation of NADH to NAD^+, requires the application of relatively high overpotentials (η=0.7 V) and confirms the relative irreversible behavior of NADH. Results also confirms the absence of any passivation of the anode when the anolyte contains only the cofactor. Taking into account that i) oxidation of the solvent starts for potentials higher than 1.2 V, and ii) there aren't other electroactive compounds, the faradaic yield of these electrolyses even those not determined, can be expected to be satisfactory.

3.4. Enzymatic oxidation of CbP by NAD^+ in a stirred discontinuous batch reactor

3.4.1. Without electrochemical regeneration of NAD^+

Batch enzymatic oxidation of CbP (reaction 1, scheme 1) was performed using the experimental setup of Fig.1, without polarization of the electrodes (without cofactor electroregeneration).

The initial concentration of the CbP (18.7 mM) corresponds to its maximum solubility in the aqueous 100 mM sodium pyrophosphate buffered solution.

Usually low (catalytic) concentrations of the cofactor NAD^+([CbP]/[NAD^+] > 10) were used to carry out the enzymatic oxidation; nevertheless, because the 'slow rate' of the involved enzymatic reaction (1), we decided to introduce NAD^+ at stoichiometric quantities (2×18.7 mM). In such conditions, CbP was completely (X=98%) converted to CbA after a reaction time of 72 h. Note that the reaction rate continuously decreases, around 10 times (2.5 mM/h→0.24 mM/h) during the duration of the reaction (72 h), whereas the evolution of the HLADH enzymatic activity showed a grace period during the first 24 h of the reaction, with a further decrease until reaching 62.5% at 72 h.

3.4.2. With electrochemical regeneration of NAD^+, (reaction 1 coupled with the reaction 2)

The enzymatic oxidation of CbP coupled with the electrooxidation of NADH (reactions 1 and 2) was carried out using the same initial concentrations of CbP (18.7 mM), NAD^+(2×18.7 mM) and HLADH (100U/cm^3). To avoid starting electrochemical regeneration of NAD^+ without NADH, the following procedure was carried out:

i) Enzymatic oxidation of CbP by NAD^+ was carried out within the anolyte storage tank, acting as a batch-stirred reactor (Fig. 1), for a duration of 30 min. After the flow of the anolyte and catholyte solutions in the microreactor started at 1 mL/min, and the I=f(E) curve was plotted Fig. 5(a) on the gold anode (to check the NADH produced by the enzymatic oxidation of the substrate CbP). The first

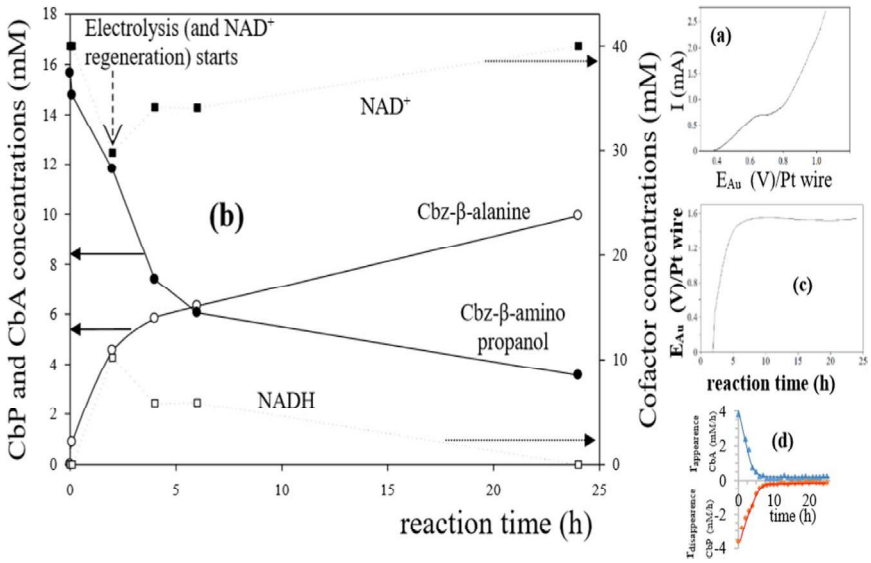

Fig. 5. Results of the overall process of "coupled enzymatic oxidation of CbP to CbA and electrochemical regeneration of NAD^+ in a filter-press microreactor". [Cbz-amino propanol]°=18.7 mM (checked by HPLC=15.7 mM, [NAD^+]°=37.4 mM; [HLADH]°=100 U/mL; 100 mM sodium pyrophosphate buffer pH 8.7. The reaction mixture (10 mL), contained in the anolyte storage tank, is stirred by a magnetic bar (Fig. 1) and thermoregulated at 25 °C. Catholyte: 100 mM sodium pyrophosphate buffer pH 8.7. **(a):** Current-potential curve plotted (on the gold using the filter-press microreactor Fig. 1) after 30 min's enzymatic reaction (1); it indicates the oxidation of NADH produced. r=5 mV/s; $Q_{anolyte}$=$Q_{catholyte}$=1 mL/min. **(b):** Temporal evolution of the concentration of the compounds involved in the oxidation of CbP by NAD^+. CbP (•), CbA (○), NAD^+(■) and NADH (□). Reaction time 0–2 h: only enzymatic oxidation (1) of the CbP arises. No flow, no current. Reaction time 2–24 h: both the enzymatic oxidation of the CbP (1) and the electrochemical generation of NAD^+ (2) take place. $I_{applied\ during\ 22\ h}$: 0.5 mA; $Q_{anolyte}$=$Q_{catholyte}$=1 mL/min. At the reaction time 2 h: [Cbz-amino propanol] ~11.9 mM; [NAD^+] ~30 mM; [HLADH] =100 U/mL. **(c):** Time dependence of the anodic potential for the electrochemical regeneration of NAD^+(coupled to the HLADH-catalyzed oxidation of Cbz-amino propanol). **(d):** chemical rate of disappearance of CbP and appearance of CbA versus time (extracted from b).

signal, observed for potentials starting at 0.4 V, exhibits a diffusional type plateau (~0.7 V, limiting current ~0.8 mA) and is attributed to the oxidation of NADH. Comparison with the current potential curve of Fig. 4 leads to the following conclusions:

- The limiting current (~0.8 mA), compared to the one in fig. 4 (~6 mA) enables the estimation of the concentration of NADH generated by the enzymatic reaction (1), for 30 min at 2.7 mM.
- The peak observed in fig. 4 (~0.69 V, ~9 mA) is absent here (Fig. 5(a), because higher volumetric flow of the anolyte prevents the concentration depletion within the electrolytic compartment and enables obtaining a constant magnitude of the current. Moreover, there is no adsorption, nor deactivation of the anode.
- For higher potentials (~0.9–1 V) the curve a, Fig. 5, presents an unidentified shoulder; this low resolution signal is absent from the I=f(E) curve of the Fig.4; it could probably correspond to a second oxidation of the NADH or to the oxidation of a product of the enzymatic reaction (1) i.e. CbA.

i) The electrodes were depolarized ($E \dashrightarrow \dashrightarrow \dashrightarrow E_{i=0}$), the flow was stopped and the enzymatic oxidation of the substrate CbP was pursued into the batch reactor for an additional 1.5 h. Concentrations of the various species contained in the reactor at this time (2 h), were indicated in Fig. 5, b: [CbP] a decrease from 18.7 (15.7 HPLC) to 11.9 mM; [NAD^+] a decrease from 2×18.7 to 30 mM and [NADH] an increase from 0 to 7 mM.

ii) The flow was restored in the microreactor and electrolysis was carried out under galvanostatic conditions, by applying a constant current of 0.5 mA (80% of the limiting current of the observed plateau, Fig. 5, a, at the time=2 h). The choice of the constant current (instead of a constant potential) enables easier operations; the Pt wire used as a pseudo reference electrode did not permit long operations without perturbations (various interferences could arise, for example, by the loss of the ionic connection by the immobilization of a bubble between the extremity of the wire and the flowing solution). The overall duration of the experiment (1)+(2) was fixed to 24 h.

The temporal evolution of the concentration of the compounds involved shown in Fig. 5(b). Starting electrolysis causes the concentration of NAD^+ to increase continuously until the end of electrolysis (t=24 h), and to practically reach its initial concentration (~37 mM, [NADH] ~0), meaning that the rate of the enzymatic oxidation of Cbz-amino propanol, is much lower than the rate of the electrogeneration of NAD^+. Note that, the instantaneously produced flux of NAD^+ is $y_f \times 0.8 \times I_{lim}/2/\ 96{,}500 = 7.5 \times 10^{-3}$ mmol/h, assuming a faradaic yield y_f ~100%. For the operating volume of the anolyte (10 cm^3), the instantaneous produced concentration of NAD^+, without consumption is 0.75 mM/h, (or $2.07.10^{-9}$ mol/s×3600 s/h×22 h×10^3 mmol/mol=0.164 m mol of NAD^+ produced during the whole operation in the overall volume of 10 cm^3). Simultaneously, the concentration of the CbP decreases until its conversion reaches 77.1% after a reaction time of 24 h.

The temporal evolution of the anode potential measured versus a platinum wire used as pseudoreference, is presented in Fig. 5(c). The curve shows that the potential reaches around 1.5 V after ~5 h of electrolysis and then it remains almost constant until the end. This value corresponds to the oxidation of water (some bubbles of O_2 were observed at the *outlet of the microreactor) and* causes the faradaic yield to decrease.

A similar conclusion was obtained by the derivatization of curves [CbP]=f(t) and [CbA]=f(t) of the Fig. 5(b); the obtained chemical rates, indicated in Fig. 5(d), become quasi nil after 5–6 h. The more acceptable explanation of the chemical rate cancellation is the complexation of HLADH with the produced aldehyde CbA; this point will discussed in the next section, but it appears that this complexation is competitive to the CbP complexation and also reversible. This is because the titration of the enzymatic activity of the HLADH does not indicate significant losses. In addition, the severe drop of the enzymatic reaction rate could explain the observed 'high value' of the anodic potential: the NAD^+ cumulates, the concentration of NADH decreases and the corresponding limiting current decreases and becomes lower than the applied current. The limitation of the chemical rate by the adsorption, on the gold (fouling of anode), of the substrate (CbP) or product (CbA) can be excluded; indeed: i) UV measurements clearly indicate that the [NADH] remains low, meaning that the enzymatic reaction (1) does not proceed; thus NAD^+ and/or other side adducts, produced by the cofactor oxidation, cumulate, and ii) after a reaction duration of 4 h, the applied current was decreased (for 30 min), from 0.5 to 0.2 mA. Meanwhile, there was no change (decrease) in the potential value (so the current was increased again to 0.5 mA).

3.4.3. Comparison of the enzymatic oxidation of CbP with and without cofactor (NAD^+) regeneration

A comparison of the enzymatic oxidation with and without cofactor regeneration is presented in Fig. 6, (I). It shows the evolution of both the substrate conversion and of the enzymatic activity of the HLADH over time. Curves a1 and a2 (X_{CbP}=f(t)) do not show differences before electrolysis (t < 2 h). Starting electrolysis (applied current= $I_{applied}$=0.5 mA) cause the regeneration of a part of the cofactor (NAD^+) and leads to an increase in the enzymatic reaction rate (in the early phase of the process) implying a higher substrate conversion than without electrolysis (at t=24 h, ΔX_{CbP} reaches 20%). The productivity was enhanced to 0.50 mM/h, the double of the value obtained in the reaction without regeneration of NAD^+.

Fig. 6, (II) presents the temporal evolution of the disappearance rate of the CbP, both with and without electrochemical regeneration of NAD^+, extracted from Fig.6, a1 and a2. Curves clearly indicate that the main changes in the chemical rate arise from reaction times of 7 h, followed the rate remaining constant and very low (r < 0.2 mM/h) for both operations. This implies that the most significant quantity of the substrate (~40%) is converted before this time.

The enzymatic activity (EA) of HLADH slightly decreases over time for both processes; without electroregeneration of NAD^+(Fig. 6, b1), the enzymatic activity loss is 4% for a duration of 24 h. In order to achieve theoretical calculations, the EA of the HLADH evolution over time will be assumed as linear, thus the following equation can be obtained:

$$[E]_{(U/L)} = [E]^\circ - 160\ t_{(h)}. \quad (5\text{-a})$$

where $[E]^\circ = 10^5$ U/L).

Operating under electrolysis (Fig. 6, b2), causes the EA of HLADH to decrease faster; losses reach ~16% for the same time and a total turnover number (TTN) of 30 was found for HLADH. As previous, the EA of the HLADH evolution over time will be assumed as linear, and the equation (5-b) can be proposed:

$$[E]_{(U/L)} = [E]^\circ - 640\ t_{(h)}. \quad (5\text{-b})$$

The observed loss in EA could be due to the polarization of the electrode, which causes a slight deactivation of the HLADH enzyme.

3.4.4. Theoretical analysis of the chemical and electrochemical reactor system

Let us consider the enzymatic reaction (1) assumed to follow the Michaelis Menten model.

$$CbP + 2\ NAD^+ + H_2O \overset{HLADH}{\Longrightarrow} 2\ NADH + CbA + 2\ H^+$$

(1, see also scheme 1)

We suppose that the HLAD enzyme (here represented by E) forms, via an equilibria, a complex with:

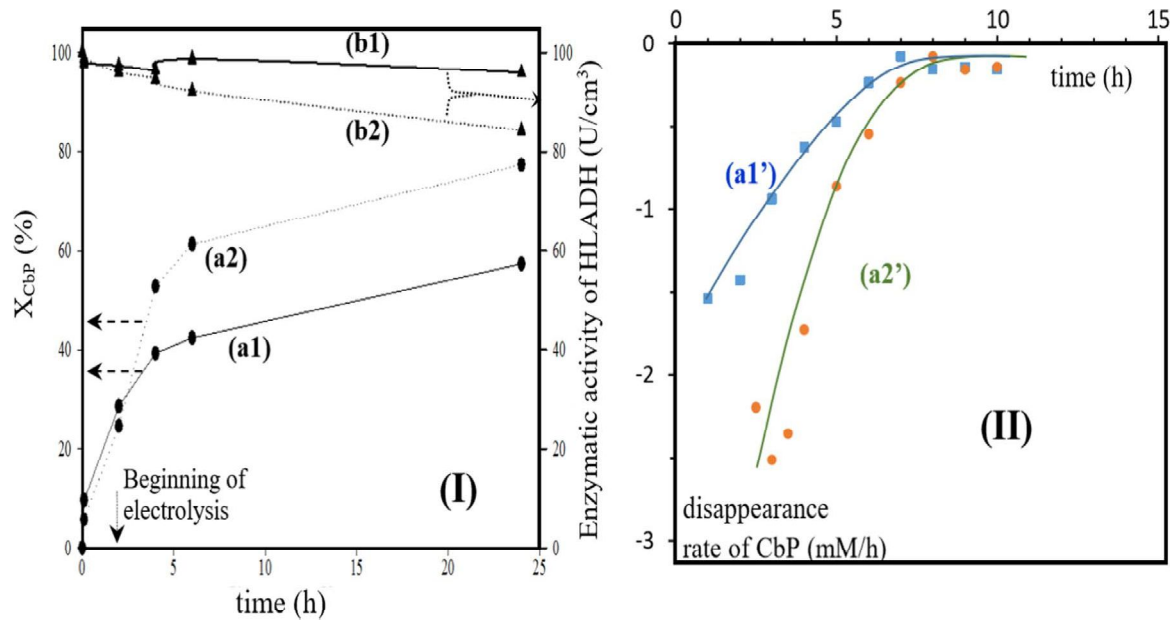

Fig. 6. Results of oxidation of CbP by NAD^+, without (a1, a1′, b1) and with (a2, a2′, b2) electroregeneration of NAD^+. **(I)** Time dependence of both the CbP conversion and the HLADH enzymatic activity, in the two cases: solid lines represent the conversion of CbP (a1) and the HLADH EA (b1) for the enzymatic oxidation without electroregeneration of NAD^+; dotted lines (a2 and b2) represent the same evolutions when the coupled oxidation was carried out with electrochemical regeneration of NAD^+. Beginning of the electrolysis at 2 h, a current of 0.5 mA was applied. Condition and operating parameters are those indicated in caption of Fig. 5. **(II)** Time dependency of the disappearance rate of CbP, without (a1′) and with (a2′) electroregeneration of NAD^+(results extracted from I, a1 and a2).

*the substrate CbP: $E + \text{CbP} \leftrightarrows \text{CbP}{-}E$ (6)

$K_6=k_{forward6}/k_{backward\ 6}=271\sim1/K_{M6}\rightarrow K_{M6}=0.0046$ M (Rodríguez-Hinestroza, 2014)

*the cofactor NAD^+: $E+NAD^+ \leftrightarrows (NAD{-}E)^+$ (7)

$K_7=k_{forward7}/k_{backward\ 7}=0.0375\ (\mu M)^{-1}\sim1/K_{M7}\rightarrow K_{M7}=26.66$ μm (Dworschack and Plapp, 1977). Note that Cleland provides values for $K_{M7}=3.9$ μm (Cleland, 1963).

*the cofactor NADH: $E + \text{NADH} \leftrightarrows (\text{NADH}{-}E)$ (8)

$K_7=k_{forward8}/k_{backward\ 8}=2.025\ (\mu M)^{-1}\sim1/K_{M8}\rightarrow K_{M8}=0.494$ μm (Dworschack and Plapp, 1977). Note that Cleland provides values for $K_{M8}=8.8$ μm (Cleland, 1963).

As a first approach, the equilibrium between the CbA product and the enzyme was not considered. The alcohol dehydrogenase must theoretically exhibit lower affinity against aldehydes (instead of the substrate). Moreover, both complexation reactions (7) and (8) must be reversible, because the enzymatic essay (Fig. 6, I, b1 and b2) does not indicate significant decreases in the enzymatic activity over time.

Thus the alcohol dehydrogenase was distributed as following:

$$[E_{initial}] = [E_{free}] + [NAD{-}E^+] + [NADH{-}E] + [CbP{-}E] \quad (9)$$

In a traditional random bi-bi model, both binary complexes CbP-E and NAD-E^+ react according to two equilibria, to lead to a ternary complex E-CbP-NAD^+. Here the reaction scheme was assumed as simpler: the reaction (10), implying binary complexes (and leading to an intermediate expected to be the ternary complex E-CbP-NAD^+) has been considered as the limiting step.

$$\text{CbP}{-}E + (\text{NAD}{-}E)^+ \rightarrow \text{intermediates} \quad (10)$$

This last assumption justifies the mass balance of the distribution of the enzyme (Eq. (9) required for calculations); indeed this equation does not include the concentration of the enzyme within the ternary complex E-CbP-NAD^+ because this adduct does not accumulate, it is assumed to decompose by faster chemical steps, releasing 2 NADH, the CbA product and 2 free enzymes E.

Taking account of the (6), (7) and (8) equilibria, the reaction (10), as well as the enzyme distribution (9) the production rate of CbA can be expressed as follows:

$$r_{(CbA)}=+\frac{d[CbA]}{dt}=\frac{k_{10}\times K_6\times K_7\times [NAD^+]\times [CbP]\times [E^\circ]^2}{(1+K_6\times [CbP]+K_7\times [NAD^+]+K_8\times [NADH])^2} \quad (11)$$

where k_{10} is the kinetic constant (L/mol/h) to be determined.

3.4.4.1. Enzymatic oxidation of CbP. The reaction (1) takes place in the stirred batch reactor (anolyte storage tank, Fig. 1), which operates at a transient state. There is no flow (nor connection) in the EμR. Taking into account that the cofactor was involved in stoichiometric conditions, then, the various concentrations could be expressed as functions of the CbP conversion X, by the following equations: $[CbP]_{overal}=[CbP]^\circ_{overal}\times(1-X)$; $[NAD^+]_{overal}=2\times[CbP]^\circ_{overal}\times(1-X)$.

Furthermore, assuming that the Eq. (11) is valid for any conversion of the substrate, and taking the enzyme stability into account (5-a), the mass balance on the CbA enables the establishment of the following expression of the conversion rate:

$$\frac{dX}{dt}=\frac{2\times k_{10}\times K_6\times K_7\times (10^5-160\times t)^2\times(1-X)^2}{\left(\frac{1}{[CbP]^\circ}+K_6\times(1-X)+K_7\times2\times(1-X)+K_8\times2\times(X)\right)^2} \quad (12)$$

where $[CbP]^\circ=0.0157$ M (determined by HPLC, for a theoretical introduced concentration of 0.018 M).

To solve this equation knowledge of the kinetic constant k_{10} is required. Matlab software is used to solve the Eq. (12) and k_{10} was estimated by fitting of the simulated concentrations of the substrate into the experimental one (results not presented here). The value that appears best fit the experiments and simulation is $k_{10}=7.5.10^{-6}$ mol/L/h for short reaction times. Nevertheless, the fit was not perfect for reactions that lasted longer than ~6 h, and as discrepancies appear, the theoretical concentration becomes lower than the experimental one. This behavior could mean that the produced adduct (CbA) is able to form a complex with the enzyme, thus implying the lowering of the available free-enzyme concentration. Consequently, we propose to take the following equilibrium into account:

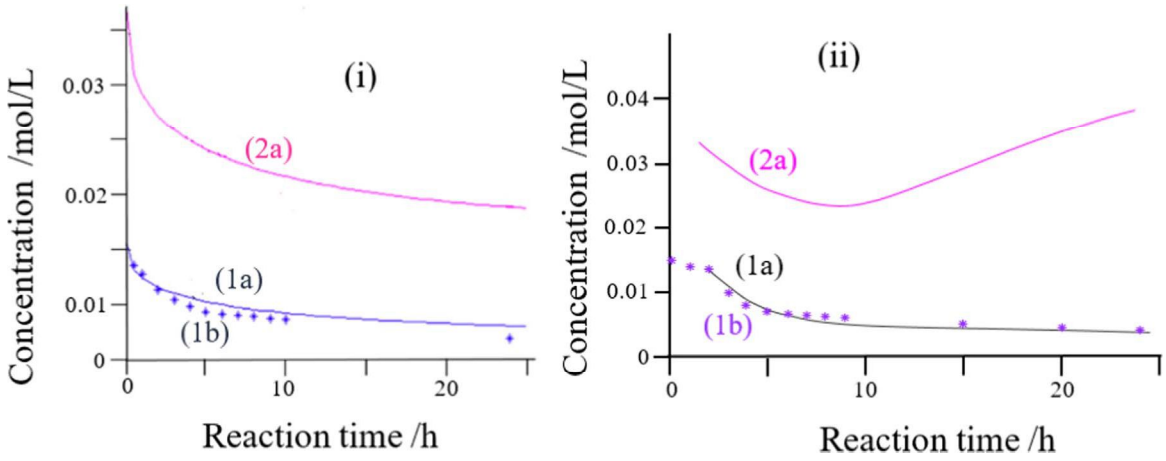

Fig. 7. Temporal evolution of the concentrations of the substrate CbP and of the NAD^+ involved in the enzymatic oxidation (1). (i) without and (ii) with electrochemical regeneration of NAD^+. Solid lines: simulated concentrations of NAD^+(Eqs. 14 and 17–18 solved by Mat Lab). Dots: experimental results extracted from fig. 6-(I)-(a1); Experimental concentration of NAD^+ was not determined. The values of the constants (k_{10}=7.5 10^{-6} L/mol/h and K_{13}=11.10^5 mol/L) were estimated by iteration allowing the best fit between experimental concentrations and theoretical calculations.

$$CbA + E \rightleftarrows CbA{-}E \tag{13}$$

$K_{13} = k_{forward\ 13}/k_{backward\ 13} \sim 1/K_{M\ 13}$ to be estimated

Note that, this complexation enzyme/product (CbA) has to be weaker compared to the complexation of the CbP substrate and also reversible, because the enzymatic assay ((Fig. 6, b1 and b2) does not indicate a significant decrease in enzymatic activity over time. In the light of these assumptions, Eq. (12) can be modified as follows:

$$\frac{dX}{dt} = \frac{2\times k_{10}\times K_6\times K_7\times (10^5-160\times t)^2\times (1-X)^2}{\left(\frac{1}{[CbP]^\circ} + K_6\times(1-X) + K_7\times 2\times(1-X) + K_8\times 2\times(X) + K_{13}\times(X)\right)^2} \tag{14}$$

Assuming that the previously determined optimal value of k_{10} =7.5 10^{-6} L/mol/h is valid, the resolution of the Eq. (14) by Matlab requires knowledge of the equilibrium constant K_{13}; this constant was iteratively estimated by fitting the simulated concentration of the substrate to the experimental one (results in Fig. 7, (i)) and its value is 1.1.10^6 L/mol.

Fig. 7(i) presents the results, i.e. simulated (solid line) and experimental (dots) temporal evolutions of the concentration of the substrate (CbP, 1a) and exhibits a good agreement especially for short reaction times. For longer durations, the observed discrepancies ($[CbP]_{exp.}$- $[CbP]_{sim.}$)/$[CbP]_{sim.}$) increase and can reach ~30%. Better knowledge of the complexation constant values will certainly allow the reduction of these discrepancies. Concerning NAD^+ only simulated concentration was presented (experimental one was not determined) and, as expected, this concentration continuously decreases.

3.4.4.2. Enzymatic oxidation of CbP coupled with the electrochemical regeneration of NAD^+. The electrochemical micro reactor EμR, operating as a plug-flow reactor, was connected to the storage tank (according to the set-up of Fig. 1) and polarized in order to perform the NAD^+ regeneration (2). The anolyte, flowing within the EμR, is continuously recycled into the anolyte storage tank, acting as a stirred batch reactor for the enzymatic reaction (1). Comparison of the volumes ratio ($V_{batch\ reactor}/V_{anolyte\ in\ the\ \mu ER}$=10/4.$10^{-2}$ cm^3 =250) enable simplifying the system and considering that the EμR operates under a 'pseudo' steady-state condition for the NADH/NAD^+ cofactor. Under galvanostatic conditions, the mass balance for NAD^+ into the EμR, at the 'pseudo' steady state, enables the following equation to be suggested:

$$Q\times([NAD+]\text{inlet of the E}\mu R - [NAD+]\text{outlet of the E}\mu R) = -\frac{I_{efficient}}{2\times F} \tag{15}$$

where Q is the volumetric flow of the mixture in the anodic compartment of the EμR and $I_{efficient}=y_f\times I_{applied}$ (y_f is the faradic yield).

The stirred batch reactor, operates at the transient state for all compounds (cofactor, substrate and product of the enzymatic reaction (1)). The mass balance for NAD^+ can be written as:

$$\frac{Q}{V}\times\left([NAD^+]_{\substack{outlet\ of\\ the\ E\mu R}} - [NAD^+]_{\substack{inlet\ of\\ the\ E\mu R}}\right) = r_{[NAD^+]\ \substack{inlet\ of\\ the\ E\mu R}} + \frac{d\,[NAD^+]_{\substack{inlet\ of\\ the\ E\mu R}}}{dt} \tag{16}$$

Assuming valid the Eq. (14) and taking into account the losses of the EA of the HLADH (Fig. 6, I, b2, and Eq. (5-b)), the mass balance for the flux of NAD^+ becomes:

$$\frac{d\,[NAD^+]_{\substack{inletof\\ theE\mu R}}}{dt} = \frac{y_f\times I_{applied}}{2\times F\times V} - \frac{2\times k_{10}\times K_6\times K_7\times [NAD^+]_{\substack{inletof\\ theE\mu R}}\times [CbP]\times (10^5-640\times t)^2}{\left(1+K_6\times[CbP] + K_7\times[NAD^+]_{\substack{inletof\\ theE\mu R}} + K_8\times[NADH]_{\substack{inletof\\ theE\mu R}} + K_{13}\times[CbA]\right)^2} \tag{17}$$

Assuming negligible the enzymatic reaction within the μER, the mass balance for the CbP into the stirred batch reactor can be written as follows:

Inlet flux-Outlet flux=0=Chemical flux+accumulation flux.

$$-\frac{d\,[CbP]}{dt} = \frac{k_{10}\times K_6\times K_7\times [NAD^+]_{\substack{inletof\\ theE\mu R}}\times [CbP]\times (10^5-640\times t)^2}{\left(1+K_6\times[CbP] + K_7\times[NAD^+]_{\substack{inletof\\ theE\mu R}} + K_8\times[NADH]_{\substack{inletof\\ theE\mu R}} + K_{13}\times[CbA]\right)^2} \tag{18}$$

The system of the Eqs. (17) and (18) was solved simultaneously, assuming valid the previously determined values of the constants and using as initial conditions:

$[CbP]^\circ = 15.\ 7\frac{m\ mol}{L}$;$[NAD^+]^\circ = 37.\ 4\frac{mmol}{L}$;

*start of the e*lectrolysis at t = 2h;.

$I_{applied}$=0.8×I_{lim}=0.5 mA (Fig. 5, a); $[NAD^+]_{inlet\ of\ the\ E\mu R\ at\ t=2\ h}$ =29.4.10^{-3} mol/L (Fig. 5 b).

The faradaic yield was not determined experimentally; on the basis of the anodic potential evolution (Fig. 5c), it seems obvious that it decreases over time, particularly for reaction times higher than 6–7 h.

Table 2
obtained values for the kinetic parameters of the enzymatic oxidation of CbP.

Reaction no.		Determined value/ unit of the constant	Michaelis constant K_{Mj} (mol/L)	Reference
(6)	E+CbP	K_6=271 L/mol	0.0046	(Rodríguez-Hinestroza, 2014)
(7)	E+NAD^+	K_7=0.037.10^6 L/mol	26.66.10^{-6}	(Dworschack and Plapp, 1977)
		K_7=0.256.10^6 L/mol	3.9.10^{-6}	(Cleland, 1963)
(8)	E+NADH	K_8=2.025.10^6 L/mol	0.494.10^{-6}	(Dworschack and Plapp, 1977)
		K_8=0.113.10^6 L/mol	8.8.10^{-6}	(Cleland, 1963)
(10)	Limiting step	2.10^{-6} < (k_{10}=7.5.10^{-6} L/mol/h) < 15.10^{-6}	–	Iterative determination, present study
(13)	E CbA	0.5.10^6 < (K_{13} =1.1.10^6 L/mol) < 2.10^6	0.91.10^{-6}	

The anodic potential indeed reaches 1.5–1.6 V/Pt wire, a relatively high value, even if this value is not rigorously defined due to the absence of a real reference electrode. Furthermore, bubbles were observed in the outlet of the anodic compartment, meaning that oxidation of water arose. To overcome the absence of information concerning the faradaic yield (under galvanostatic conditions), the following calculation method was applied:

From the limiting current of the NAD^+ oxidation (Fig. 5, (a)) we access the proportionality constant ξ: $I_{lim.\ at\ 2\ h}=(nFSD/\delta)\times[NAD^+]_{inlet\ of\ the\ E\mu R\ at\ t=2\ h}=\xi\times[NAD^+]_{inlet\ of\ the\ E\mu R\ at\ t=2\ h}$.

Knowing the $[NAD^+]_{inlet\ of\ the\ E\mu R\ at\ t=2\ h}$ =29.4.10^{-3} mol/L (Fig. 5, b), ξ can be deduced and its value is 0.0235 A.L/mol. Taking into account the instantaneous concentration of the cofactor, determined iteratively from the resolution of the system of Eqs. (17) and (18), the following test was added in the Matlab:

$$\text{if } (\xi \times [NAD^+]_{\text{inlet of the } E\mu R\ (t)}) \geq 0.5.10^{-3}\ \text{A } (=I_{applied} = 0.8 \times I_{lim}),$$

$$\text{then } I_{efficient\ (t)} = I_{applied};$$

$$\text{if not, then } I_{efficient\ (t)} = I_{applied} - \xi \times [NAD^+]_{\text{inlet of the } E\mu R\ (t)}.$$

The results obtained by the resolution of the system of Eq. (17 and 18), using k_{10} =7.5×10^{-6} L/mol/h and K_{13}=11×10^5 mol/L, were presented in Fig. 7 (ii) 'as solid lines' for the CbP and the NAD^+, comparatively to the experimental results (dots) for the substrate. Comparison of simulated and experimental concentrations of the CbP leads to a satisfactory agreement. The simulated curve of concentration of the CbP is slightly higher or lower that the experimental one, and the observed discrepancies were attributed to the experimental uncertainties of the concentrations determinations (HPLC).

Concerning the NAD^+ only simulated concentrations were presented, experimental ones were not determined; as expected, the simulated concentration decreases at the beginning of the electrolysis (t=2 h) due to the low concentration of NADH; at this time the electrochemical rate of regeneration of NADH is low, implying a low initial faradic yield due to the galvanostatic operation. For higher reaction times (~7 h), the enzymatic reaction generates sufficient quantities of NADH, followed by the electrochemical regeneration rate of NAD^+ increasing and consequently the theoretical curve also.

To sum up, these results (especially the values of the various constants summarized in Table 2) can be assumed sufficiently reliable to enable the design of an electrochemical reactor in order to ensure any required productions of the CbA.

3.5. Enzymatic oxidation of CbP in a Fed-batch reactor

To maintain high CbA productivity, the rate of the enzymatic reaction (1) must remain high, implying high concentrations of the CbP. We choose here to carry out the oxidation of CbP by sequentially adding the substrate into the stirred reactor (fed-batch mode), expecting the restoration of its initial concentration ([CbP]°=18.7 mM=maximum solubility). This way enables the operation with CbP in sufficient quantities to create competition between equilibria 6 and 13; fresh substrate allow the release of the enzyme from the CbA-E complex (13) and the complexation (6) to take place, thus enabling the enzymatic reaction (1) to arise. Fed-batch is a solution that helps to enables overcoming the low solubility of the substrate and increasing productivity.

3.5.1. Without cofactor (NAD^+) regeneration

The rate of the enzymatic reaction (1) also depends on the concentration of NAD^+. In this section, experiments were performed using concentration that were three-fold higher (112.2 mM) than the stoichiometric quantity required (2*18.7 mM). Fig. 8 presents the temporal evolution of the mole number (*instead of concentration, because the changes in the reaction mixture volume: CbP additions +aliquots taken for analyses*) of both CbP and CbA, for long reaction times (~4 days). Three pulses of the substrate were introduced into the reactor (✦ 0.025 mmol/addition, each one corresponding to an increase of the CbP concentration of 5 mmol/L).

The molar quantity of CbP decreases over time for all experiments and increases after each pulse, thus its 'average' molar quantity remains practically constant (~0.06 mmol), enabling satisfactory chemical rates for the reaction (1). The curve providing the produced mole number of CbA appears to be a monotonously increasing function, without significant lowering in the production rates, due to the fed-batch reactor. The produced quantity of CbA corresponds to 88.4% (chemical selectivity) of CbP converted during 96 h of reaction, which leads to a final produced flux of CbA 1.55×10^{-6} mol/h.

The produced quantity of CbA at 72 h reaches 0.1383 m mol, corresponding to an average flux of 1.92.10^{-6} mol/h, *(which represents a conversion of ~82% of the total quantity of CbP introduced: 0.168 mmol)*; this flux of CbA is compared to the flux previously (§3.4.1.) obtained at the same reaction time, i.e. 1.27.10^{-6} mol/h (or

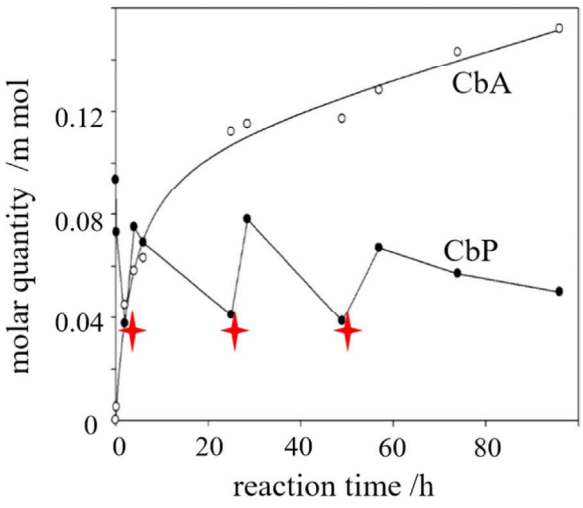

Fig. 8. Temporal evolution of concentration of both the substrate (CbP, (•)) and the product (CbA (○)) in the fed-batch chemical reactor. [CbP]°=18.7 mM (15.7 mmol/L detected by HPLC); [NAD^+]°=112.2 mM; 100 mM sodium pyrophosphate buffer pH 8.7; 100 U/mL of HLADH; V=5 mL ; T=25 °C ; reaction time : 96 h. Three additions of solid CbP were carried out at 3, 25.5 and 45.5 h; ✦ 0.025 mmol of substrate added, each one corresponding to an increase of the CbP concentration in the reactor of 5 mmol/L; total amount of CbP added=0.168 m mol; final amount of CbA produced=0.149 m mol.

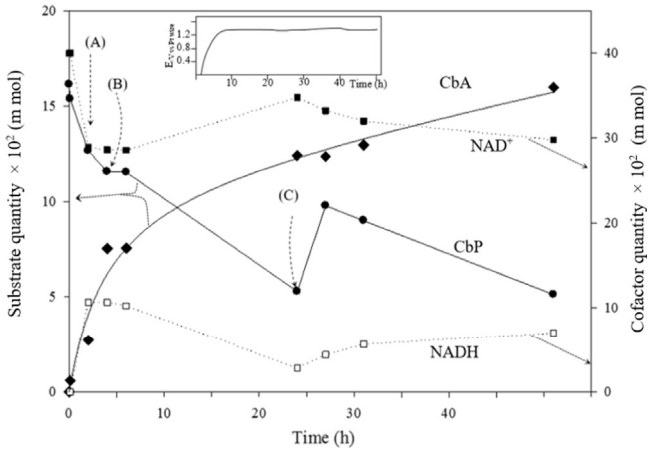

Fig. 9. Results of the overall process of "coupled enzymatic oxidation of CbP to CbA and electrochemical regeneration of NAD^+ in a filter-press microreactor". [Cbz-amino propanol]°=18.7 mM (checked by HPLC=15.7 mM, $[NAD^+]°$=37.4 mM; [HLADH]°=100 U/mL; 100 mM sodium pyrophosphate buffer pH 8.7. The reaction mixture (10 mL), contained in the anolyte storage tank, is stirred by a magnetic bar (Fig. 1) and thermoregulated at 25 °C. Catholyte: 100 mM sodium pyrophosphate buffer pH 8.7. Enzymatic reaction overall duration=51 h. **(A)**: Beginning of the **e**lectrolysis (and NAD^+ regeneration) starts under galvanostatic conditions (0.5 mA)**; (B) and (C):** addition of 5 mM of solid CbP in the anolyte at t=4 h and 24 h respectively. (•): CbP quantity; (♦): CbP conversion; (■): NAD^+; (□): NADH. **Inset:** Time dependence of the anodic potential for the electrochemical regeneration of NAD^+(coupled to the HLADH-catalyzed oxidation of Cbz-amino propanol). Electrolysis duration: from 2 h until 51 h at 0.5 mA. T=25 °C; $Q_{anolyte}=Q_{catholyte}$=1 mL/min. Catholyte: 100 mM sodium pyrophosphate buffer pH 8.7.

0.092 mmol, corresponding to a conversion of 98% of the initial quantity of CbP). This comparison clearly shows an enhancement of the CbA production of about 50% due to the sequential additions of the substrate. Besides, the initial reaction rate of the production of CbA (Fig. 8) was 4.2 mM/h, which is 1.7 times higher than the rate obtained in the batch mode. This was as expected, due to the higher initial NAD^+ concentration. As a consequence of the high initial reaction rate, the first addition of the substrate was performed after 3 h of reaction, while the other two additions were performed at 25.5 and 49 h.

3.5.2. With electrochemical regeneration of NAD^+

The enzymatic oxidation of CbP (1) coupled with the electrochemical cofactor regeneration (2) was performed with two additions of substrate for the same conditions as in 3.5.1., except for the cofactor amount. This latter was introduced at 37.4 mM, three times lower than the reaction without regeneration. As previously mentioned (3.4.4.2.), the gold anode was polarized 2 h after the beginning of the enzymatic oxidation and the results were shown in Fig. 9, with the temporal evolution of the anodic potential indicated in the inset. The first addition of 5 mM of solid CbP in the anolyte was achieved after a reaction time of 4h,

while the second addition at t=24 h. Between two pulses, the concentration of CbP first decreases then increases immediately after; this implies the enhancement of the rate of the enzymatic reaction, simultaneously affecting the cofactor concentration. Between two pulses, the concentration of CbP first decreases then increases immediately after; this implies the enhancement of the rate of the enzymatic reaction, simultaneously affecting the cofactor concentration. Indeed, for reaction times of 4–5 h, both the concentrations of NADH and NAD^+ remain quasi stable, meaning that the flux of the anodic oxidation (2), and the enzymatic oxidation (1) have similar magnitudes. The NADH concentration decreases until 24 h, translating a lowering of the rate of the enzymatic oxidation, in comparison to the electrochemical one (which remains constant).

After the second addition of the CbP, the NADH concentration slightly increases and remains constant. Note that without addition of the substrate (Fig. 5, for t > 2 h), the NADH concentration falls monotonously. Substrate conversion X to CbA (calculated versus the total mole of CbP added) continuously increases, ~40% and 80%, respectively at 6 and 51 h.

Even if this final conversion is similar to that obtained with the fed-batch reactor without NAD^+ regeneration (88.4% at 96 h, Fig. 8), a gain of 45 h is observed in the present case; moreover, the initial concentration involved of the cofactor is 37.4 mM instead 118 mM used in electrolysis described in Fig. 8.

The productivity of the CbA obtained at 51 h was a little lower (0.44 mM/h) than the one obtained without NAD^+ regeneration (0.56 mM/h, §**3.5.1.**). However, in this last operation three substrate pulses were added (instead of two) and the initial concentration of NAD^+ is three times that of the required one.

The obtained TTN was 56, which is higher than the one obtained in the batch configuration, taking into account that the reaction time was longer. Finally, it is worth mentioning that direct electrochemical regeneration does not significantly affect the stability of the HLADH enzyme; the fed-batch reaction efficiently operates for several days, with only one separation stage being required to recover the cofactor NAD^+.

4. Conclusions

Direct electrochemical regeneration of NAD^+ was demonstrated since NADH can be directly oxidized to NAD^+ on a gold anode using a filter-press microreactor. Its high specific area (250 cm^{-1}) enables high (92%) conversion of NADH to NAD^+. No significant fouling of the electrode was observed nor deactivation of the pyridinic cofactor (no side products/HPLC), even if high potentials (1 V/vs Pt wire) were applied.

The enzymatic oxidation of CbP in the presence of HLADH was studied as a reaction model; the results show that the chemical rate is almost cancelled after a few hours (5–7) due to the complexation of the enzyme by the produced aldehyde CbA. Long reaction times (~3 days) were required to reach quasi-quantitative conversion (98%) of the substrate.

The electrochemical regeneration of NAD^+ was successfully coupled with the HLADH-catalyzed oxidation of CbP for the production of CbA, as proof of the concept 'to use the microreactor/coupled with enzymatically assisted indirect electrochemical oxidation'. Thus, coupling electrochemistry to the chemistry enables reducing the reaction time (77% after the fixed reaction time of 24 h). Nevertheless complexation of the enzyme by the product (CbA) appears to introduce a serious drawback on the overall processes. Sequential additions of the substrate, maintaining its concentration high, enabling to create competition between the equilibrium of substrate and product complexation, and consequently to release the enzyme and to allow its availability against the substrate. Results, summarized in Table 3, were very positive, especially for enzymatic oxidation coupled with the electrochemical regeneration (increasing conversion and productivity). Another solution to limit the HLADH complexation by the product could be its continuous removal from the solution, and this will constitutes a future work.

Simulation of the system was carried out assuming the bimolecular reaction between complexes of substrate-Enzyme and $(NAD\text{-enzyme})^+$ as the limiting step. Iterative determination of both the kinetic constant and the CbA-HLADH equilibrium constant was performed by fitting the theoretical temporal evolution of the concentration of the substrate with the experimental one; the determined values (Table 2) allows designing the system for a certain production. Finally, the proposed system is effective since it is not an invasive method and it was proven that it efficiently oxidizes the NADH to NAD^+ and uses it, in situ, for the oxidation of valuable chemicals.

Table 3
Oxidation of CbP to CbA catalyzed by HLADH. 18.7 mM CbP, HLADH activity of 100 U/mL, pH 8.7 and 25 °C were used in all the cases.

Configuration	NAD^+ electrochemical regeneration	NAD^+ initial concentration (mM)	Reaction time (h)	Conversion CbP (%)	Productivity (mM CbA/h)	TTN
Batch	–	37.4	24	58	0.24	0.5
Batch	√	37.4	24	77	0.50	30
Fed-batch	–	112.2	50	88.4	0.56	0.5
Fed-batch	√	37.4	51	80.4	0.44	56

Acknowledgements

This work was supported by the Spanish MICINN, Project no. CTQ2011-28398-CO2-01. The authors from UAB are members of the Research group 2014SGR452 and Biochemical Engineering Unit of the Reference Network in Biotechnology (XRB), Generalitat de Catalunya.

References

Aizawa, M., Coughlin, R.W., Charles, M., 1975. Electrochemical regeneration of nicotinamide adenine dinucleotide. Biochim. Et. Biophys. Acta (BBA)-Gen. Subj. 385, 362–370.

Andersson, L., Wolfenden, R., 1982. A general method of α-aminoaldehyde synthesis using alcohol dehydrogenase. Anal. Biochem. 124, 150–157.

Ardao, I., Alvaro, G., Benaiges, M.D., 2011. Reversible immobilization of rhamnulose-1-phosphate aldolase for biocatalysis: enzyme loading optimization and aldol addition kinetic modeling. Biochem. Eng. J. 56, 190–197.

Blaedel, W., Jenkins, R.A., 1975a. Electrochemical oxidation of reduced nicotinamide adenine dinucleotide. Anal. Chem. 47, 1337–1343.

Blaedel, W., Jenkins, R.A., 1975b. Electrochemical oxidation of reduced nicotinamide adenine dinucleotide. Anal. Chem. 47, 1337–1343.

Cantet, J., Bergel, A., Comtat, M., 1996. Coupling of the electroenzymatic reduction of NAD^+ with a synthesis reaction. Enzym. Microb. Technol. 18, 72–79.

Cheikhou, K., Tzedakis, T., 2008. Electrochemical microreactor for chiral syntheses using the cofactor NADH. AIChE J. 54, 1365–1376.

Chenault, H.K., Simon, E.S., Whitesides, G.M., 1988. Cofactor regeneration for enzyme-catalysed synthesis. Biotechnol. Genet. Eng. Rev. 6, 221–270.

Cheng, R.P., Gellman, S.H., DeGrado, W.F., 2001. β-Peptides: from structure to function. Chem. Rev. 101, 3219–3232.

Choban, E., Waszczuk, P., Tzedakis, T., Kenis, P., Yoon, S., and Kane, C., 2007. Microfluidic Device and Synthetic Methods. *U.S. Patent 7* 273 541.

Cleland, W.W., 1963. The kinetics of enzyme-catalyzed reactions with two or more substrates or products: I. Nomenclature and rate equations. Biochim. Et. Biophys. Acta (BBA) – Spec. Sect. Enzymol. Subj. 67, 104–137.

Dalziel, K., 1961. Preparation and properties of crystalline alcohol dehydrogenase from liver. Biochem. J. 80, 440–445.

Dalziel, K., Dickinson, F., 1965. Aldehyde mutase. Nature 206, 255–257.

van der Donk, W.A., Zhao, H., 2003. Recent developments in pyridine nucleotide regeneration. Curr. Opin. Biotechnol. 14, 421–426.

Dworschack, R.T., Plapp, B.V., 1977. Kinetic of N ative and activated isozymes of horse liver alcohol dehydrogenase. Biochemistry 16 (1), 111–116.

Ege, M., Wanner, K.T., 2008. Diastereoselective synthesis of β-amino acid derivatives from dihydropyridones. Tetrahedron 64, 7273–7282.

Gorton, L. Domínguez, E., 2007. Electrochemistry of $NAD(P)^+$/NAD(P)H. In: Encyclopedia of Eelectrochemistry, Published Online: Wiley Online Library.

Hald, E., Lehmann, P., Ziegenhorn, J., 1975. Molar Absorptivities of β-NADH and β-NAD^+ at 260 nm. Clin. Chem. 21, 884–887.

Hinson, J.A., Neal, R.A., 1975. An examination of octanol and octanal metabolism to octanoic acid by horse-liver alcohol dehydrogenase. Biochim. Et. Biophys. Acta (BBA)-Enzymol. 384, 1–11.

Hollmann, F., Hofstetter, K., Schmid, A., 2006. Non-enzymatic regeneration of nicotinamide and flavin cofactors for monooxygenase catalysis. Trends Biotechnol. 24, 163–171.

Hollmann, F., Arends, Isabel W.C.E., Buehler, Katja, 2010. Biocatalytic redox reactions for organic synthesis: nonconventional regeneration methods. ChemCatChem 2 (7), 762–782.

Hummel, W., Kula, M.R., 1989. Dehydrogenases for the synthesis of chiral compounds. Eur. J. Biochem. 184, 1–13.

Iwuoha, E.I., Smyth, M.R., 2003. Reactivities of organic phase biosensors: 6. Square-wave and differential pulse studies of genetically engineered cytochrome $P450_{cam}$ (CYP101) bioelectrodes in selected solvents. Biosens. Bioelectron. 18, 237–244.

Jaegfeldt, H., 1981. A study of the products formed in the electrochemical reduction of nicotinamide-adenine-dinucleotide. J. Electroanal. Chem. Interfacial Electrochem. 128, 355–370.

Juaristi, E., Lopez-Ruiz, H., 1999. Recent advances in the enantioselective synthesis of -amino acids. Curr. Med. Chem. 6, 983–1004.

Kane, C., 2005. Conception et réalisation de microréacteurs électrochimiques – Application à la régénération électroenzymatique de NADH et potentialités en synthèse. Université Paul Sabatier – Toulouse III, Toulouse, France.

Kochius, S., Magnusson, A.O., Hollmann, F., Schrader, J., Holtmann, D., 2012. Immobilized redox mediators for electrochemical $NAD(P)^+$ regeneration. Appl. Microbiol. Biotechnol. 93, 2251–2264.

Liu, M., Sibi, M.P., 2002. Recent advances in the stereoselective synthesis of β-amino acids. Tetrahedron 58, 7991–8035.

Moiroux, J., Elving, P.J., 1980. Mechanistic aspects of the electrochemical oxidation of dihydronicotinamide adenine dinucleotide (NADH). J. Am. Chem. Soc. 102, 6533–6538.

Pohar, A., Plazl, I., 2009. Process intensification through microreactor application. Chem. Biochem. Eng. Q. 23, 537–544.

Rodríguez-Hinestroza, R.A., July 2014. Ph.D. in Biotechnology. Universitat Autònoma de Barcelona. Barcelona, Spain.

Rudat, J., Brucher, B.R., Syldatk, C., 2012. Transaminases for the synthesis of enantiopure beta-amino acids. AMB Express 2, 11.

Samec, Z., Elving, P.J., 1983. Anodic oxidation of dihydronicotinamide adenine dinucleotide at solid electrodes; mediation by surface species. J. Electroanal. Chem. Interfacial Electrochem. 144, 217–234.

Samec, Z., Elving, P.J., 1983. Anodic oxidation of dihydronicotinamide adenine dinucleotide at solid electrodes; mediation by surface species. J. Electroanal. Chem. Interfacial Electrochem. 144, 217–234.

Steer, D.L., Lew, R.A., Perlmutter, P., Ian, S.A., Aguilar, M.-I., 2002. β-amino acids: versatile peptidomimetics. Curr. Med. Chem. 9, 811–822.

Tudorache, M., Mahalu, D., Teodorescu, C., Stan, R., Bala, C., Parvulescu, V.I., 2011. Biocatalytic microreactor incorporating HRP anchored on micro-/nano-lithographic patterns for flow oxidation of phenols. J. Mol. Catal. B: Enzym. 69, 133–139.

Tzedakis, T., Cheikhou, K., Jerôme, R., Karine, G.S., Olivier, R., 2010. Electrochemical study in both classical cell and microreactors of flavin adenine dinucleotide as a redox mediator for NADH regeneration. Electrochim. Acta 55, 2286–2294.

Tzedakis, T., Kane, C., Launay, 2006. A. Method for Electrochemical Reaction and Electrochemical Reactor with Microchannels and Method for Making Same. WO Patent 2,006,053,962.

Tzedakis, T., Kane, C., Launay, A., 2004. French Patent, n (04.12305, 2004).

Yoon, S.K., Choban, E.R., Kane, C., Tzedakis, T., Kenis, P.J., 2005. Laminar flow-based electrochemical microreactor for efficient regeneration of nicotinamide cofactors for biocatalysis. J. Am. Chem. Soc. 127, 10466–10467.

Zhao, H., van der Donk, W.A., 2003. Regeneration of cofactors for use in biocatalysis. Curr. Opin. Biotechnol. 14, 583–589.